Three-body calculations of the triple-α reaction

S. Ishikawa*

Science Research Center, Hosei University, 2-17-1 Fujimi, Chiyoda, Tokyo 102-8160, Japan

(Received 16 December 2012; revised manuscript received 9 March 2013; published 13 May 2013)

Recently, the triple-α (3α) process, by which three ^{4}He nuclei are fused into a ^{12}C nucleus in stars, was studied by using different methods to solve the quantum mechanical three-body problem. The results for the thermonuclear reaction rate for the process differ by several orders at low stellar temperatures of 10^7–10^8 K. In this paper, we will present calculations of the 3α process by using a modified Faddeev three-body formalism in which the long-range effects of Coulomb interactions are accommodated. The reaction rate of the process is calculated via an inverse process: three-alpha (3-α) photodisintegration of a ^{12}C nucleus. The calculated reaction rate is about 10 times larger than that of the Nuclear Astrophysics Compilation of Reaction Rates at 10^7 K and is notably smaller than the results of recent three-body calculations. We will discuss a possible reason for the difference.

DOI: 10.1103/PhysRevC.87.055804 PACS number(s): 26.20.Fj, 21.45.−v, 24.10.−i, 25.20.−x

I. INTRODUCTION

The thermonuclear reaction rate of the triple-α (3α) process is known to be important input to studies of stellar nucleosynthesis and stellar evolution (see, e.g., Refs. [1,2]). This process at stellar temperatures as high as 10^9 K (the resonant region) is dominated by a sequential process in which successive formations of the 2-α resonant state, e.g., ^{8}Be(0^+_1), and then the three-alpha (3-α) resonant state, e.g., ^{12}C(0^+_2) (the Hoyle state) play the essential role [3,4]. On the other hand, at lower temperatures of 10^7 K, where kinematical energies of α particles are not high enough to produce the ^{8}Be(0^+_1) resonance as a doorway state, the process is nonresonant and should be considered as a direct three-body reaction. The Nuclear Astrophysics Compilation of Reaction Rates (NACRE) 3α reaction rate [5] is evaluated by adapting the sequential process with extensions of the resonance formula to low energies under the assumption of energy-dependent widths [6,7] as a simulation of the direct reaction.

Because of recent developments in solving the Schrödinger equations for three-body continuum states numerically, there appeared some three-body calculations of the 3α reaction rate. Ogata *et al.* [8] have first calculated the 3α reaction rate by solving the 3-α Schrödinger equations by using the continuum-discretized coupled-channel (CDCC) method, in which a three-body wave function is expanded by a set of discretized α-α scattering states. (Hereafter their rate is referred to as the OKK rate.) Due to huge differences from the NACRE rate at low temperatures (see Fig. 4 below), the OKK rate was reported to have significant effects on stellar evolutionary phenomena [9–15]. Recently, calculations in which 3-α continuum states are treated by using the hyperspherical harmonics method combined with the R-matrix method was performed in Refs. [16,17] (HHR rate). In Refs. [18,19], the present author reported some results of the 3α reaction rate calculated by using the Faddeev three-body formalism [20] modified so that effects of long-range Coulomb interactions are accommodated, which has been successfully applied to the study three-nucleon scattering systems [21,22]. More recently, a method of imaginary time [23] has been applied to calculate the 3α reaction rate [24]. While these different calculations agree with each other and with the NACRE rate in the resonant region, they differ considerably at lower temperatures (see Fig. 4 below).

This paper will describe some details of the calculations of the 3α reaction rate partially reported in Refs. [18,19] and will discuss the differences among the calculations. In the following, after a formalism to calculate the reaction rate is described in Sec. II, results of calculations will be presented in Sec. III. In Sec. IV, to understand the differences between the present calculations and those of others, CDCC calculations will be performed. A summary will be given in Sec. V.

II. FORMALISM

A. Basic formalism

We consider a system of three α particles 1, 2, and 3, and use Jacobi coordinates $\{\boldsymbol{x}_i, \boldsymbol{y}_i\}$ to describe the three-body system defined as

$$\begin{aligned} \boldsymbol{x}_i &= \boldsymbol{r}_j - \boldsymbol{r}_k, \\ \boldsymbol{y}_i &= \boldsymbol{r}_i - \tfrac{1}{2}(\boldsymbol{r}_j + \boldsymbol{r}_k), \end{aligned} \tag{1}$$

where (i, j, k) denotes (1, 2, 3) or its cyclic permutations, and $\boldsymbol{r}_i$ is the position vector of particle i. Momenta conjugate to $\boldsymbol{x}_i$ and $\boldsymbol{y}_i$ are denoted by $\boldsymbol{q}_i$ and $\boldsymbol{p}_i$, respectively. Subscripts to indicate particles will be omitted when there is no confusion.

Let us consider the electric quadrupole ($E2$) transition from a 3-α continuum state of the total angular momentum 0 to the ^{12}C(2^+_1) bound state emitting a photon of energy

$$E_\gamma = E - E_b = E + |E_b|, \tag{2}$$

where E is the total energy of the 3-α continuum state in the center-of-mass system and E_b is the energy of the ^{12}C(2^+_1) state with respect to the 3-α threshold energy. The transition

*E-mail: ishikawa@hosei.ac.jp

amplitude for the process is given by

$$F^{(\mathrm{B})}(q,\hat{\boldsymbol{x}},\hat{\boldsymbol{y}}) = \langle \Psi_b | H_\gamma | \boldsymbol{q},\boldsymbol{p}\rangle^{(+)}, \tag{3}$$

where H_γ is the electromagnetic transition operator, Ψ_b is the 3-α bound-state wave function of the $^{12}\mathrm{C}(2_1^+)$ state, and $|\boldsymbol{q},\boldsymbol{p}\rangle^{(+)}$ is the 3-α continuum state initiated by a free 3-α state $|\boldsymbol{q},\boldsymbol{p}\rangle$ with the outgoing boundary condition.

The initial momenta, $\boldsymbol{q}$ and $\boldsymbol{p}$, take a variety of values as far as satisfying the energy conservation relation

$$E = \frac{\hbar^2}{m_\alpha} q^2 + \frac{3\hbar^2}{4m_\alpha} p^2, \tag{4}$$

where m_α is the mass of the α particle. To avoid a cumbersome procedure to calculate all $|\boldsymbol{q},\boldsymbol{p}\rangle^{(+)}$ states, we calculate the inverse reaction of the 3α reaction, namely, the $E2$ photodisintegration of $^{12}\mathrm{C}(2_1^+)$:

$$^{12}\mathrm{C}(2_1^+) + \gamma \to \alpha + \alpha + \alpha. \tag{5}$$

By using the disintegration cross section of this process, $\sigma_\gamma(E_\gamma)$, the 3α reaction rate $\langle\alpha\alpha\alpha\rangle$ at stellar temperature T is calculated (see, e.g., Ref. [25]) from

$$\langle\alpha\alpha\alpha\rangle = (3)^{3/2} 240\pi \left(\frac{\hbar}{m_\alpha c}\right)^3 \frac{c}{(k_\mathrm{B}T)^3} e^{-\frac{E_b}{k_\mathrm{B}T}} \times \int_{|E_b|}^{\infty} E_\gamma^2 \sigma_\gamma(E_\gamma) e^{-\frac{E_\gamma}{k_\mathrm{B}T}} dE_\gamma, \tag{6}$$

where k_B is the Boltzmann constant. Note that we apply nonrelativistic kinematics for the 3-α systems and that we do not consider a capture to the $^{12}\mathrm{C}$ ground state directly by an electron-positron pair emission in the present work as in other works [8,16,17].

The three-body disintegration reaction is calculated by defining a wave function [26] in an integral equation form,

$$|\Psi\rangle = \frac{1}{E + \imath\epsilon - H_{3\alpha}} H_\gamma |\Psi_b\rangle, \tag{7}$$

or in a differential equation form,

$$(E - H_{3\alpha})\,|\Psi\rangle = H_\gamma |\Psi_b\rangle, \tag{8}$$

where $H_{3\alpha}$ is the Hamiltonian of the 3-α system.

The asymptotic form of the wave function evaluated by using the saddle-point approximation [27] is a purely outgoing wave in three-body space with amplitude $F^{(\mathrm{B})}$,

$$\Psi(\boldsymbol{x},\boldsymbol{y}) \underset{\substack{x\to\infty \\ y/x \text{ fixed}}}{\to} \frac{e^{\imath\left(K_0 + \mathcal{O}(R^{-1})\right)R}}{R^{5/2}} F^{(\mathrm{B})*}(q,\hat{\boldsymbol{x}},\hat{\boldsymbol{y}}), \tag{9}$$

where the hyperradius R and momentum K_0 are given by

$$R = \sqrt{x^2 + \frac{4}{3}y^2} \tag{10}$$

and

$$K_0 = \sqrt{\frac{m_\alpha}{\hbar^2}E}, \tag{11}$$

q is calculated from the following relation:

$$q = \frac{1}{\sqrt{1 + \frac{4}{3}\frac{y^2}{x^2}}} K_0, \tag{12}$$

and long-range terms due to the Coulomb interaction [22] are expressed just by $O(R^{-1})$ for simplicity.

The photodisintegration cross section is given by the breakup amplitude as

$$\sigma_\gamma(E_\gamma) = \frac{1}{20\pi}\frac{\hbar}{m_\alpha c}\frac{1}{K_0^3}\left(\frac{3}{4}\right)^2 \times \int_0^{K_0} dq\, q^2 p |F^{(\mathrm{B})}(q,\hat{\boldsymbol{x}},\hat{\boldsymbol{y}})|^2. \tag{13}$$

We write the 3-α Hamiltonian as

$$H_{3\alpha} = H_0 + \sum_{i=1}^{3} V_i + W, \tag{14}$$

where H_0 is the internal kinetic energy operator of the three-body system, V_i is a two-body potential (2BP) to describe the interaction between particles j and k consisting of a short-range nuclear potential $V_i^{\mathrm{S}}(x_i)$ and the Coulomb potential $V^{\mathrm{C}}(x_i)$ with $Z = 2$:

$$V_i = V^{\mathrm{S}}(x_i) + V^{\mathrm{C}}(x_i) = V^{\mathrm{S}}(x_i) + \frac{(Ze)^2}{x_i}, \tag{15}$$

and W is a 3-α potential (3BP). Details of potentials used in this work will be described in the next section.

A partial-wave decomposition is performed by introducing an angular function,

$$|\theta(\hat{\boldsymbol{x}},\hat{\boldsymbol{y}})) = [Y_L(\hat{\boldsymbol{x}}) \otimes Y_\ell(\hat{\boldsymbol{y}})]^J_M, \tag{16}$$

where $\boldsymbol{L}$ denotes the relative orbital angular momentum of the pair of particles, $\boldsymbol{\ell}$ is the orbital angular momentum of the spectator particle, and $\boldsymbol{J}(= \boldsymbol{L} + \boldsymbol{\ell})$ and M are the total angular momentum of the three particles and its third component, respectively. A set of quantum numbers (L,ℓ,J,M) is represented by the index θ.

B. Faddeev method

Now, we consider applying a modified version of the Faddeev three-body method [20] to solve Eq. (7), in which we take into account the long-range property of Coulomb interactions [28]. Here, we introduce an auxiliary Coulomb potential $u^{\mathrm{C}}_{i,j}(y_i)$ that acts between the center of mass of the pair (j,k) and the spectator i with respect to the charges of the pair (i,j),

$$u^{\mathrm{C}}_{i,j}(y_i) = \frac{(Ze)^2}{y_i}. \tag{17}$$

Together with the similarly defined $u^{\mathrm{C}}_{i,k}(y_i)$, we introduce a Coulomb potential

$$u^{\mathrm{C}}_i(y_i) = u^{\mathrm{C}}_{i,j}(y_i) + u^{\mathrm{C}}_{i,k}(y_i) = \frac{2(Ze)^2}{y_i}. \tag{18}$$

In Faddeev theory, a three-body wave function Ψ is decomposed into three (Faddeev) components:

$$\Psi = \Phi^{(1)} + \Phi^{(2)} + \Phi^{(3)}. \tag{19}$$

Corresponding to this decomposition, the three-body potential and the electromagnetic operator are decomposed into three components:

$$W = W_1 + W_2 + W_3 \tag{20}$$

and

$$H_\gamma = H_{\gamma,1} + H_{\gamma,2} + H_{\gamma,3} \tag{21}$$

with the condition that W_i and $H_{\gamma,i}$ are symmetric with respect to the exchange of j and k.

The modified Faddeev equations [26,28] read

$$\Phi^{(1)} = \mathcal{G}_1(E) H_{\gamma,1} |\Psi_b\rangle + \mathcal{G}_1(E)\,[\Delta\Phi]^{(1)} \quad \text{(and cyclic permutations)}, \tag{22}$$

where the operator $\mathcal{G}_i(E)$ is a channel Green's function defined as

$$\mathcal{G}_i(E) \equiv \frac{1}{E + \imath\varepsilon - H_0 - V_i - u_i^{\mathrm{C}}}, \tag{23}$$

and we use the shorthand notation

$$[\Delta\Phi]^{(1)} \equiv \left(V_1 - u_{2,3}^{\mathrm{C}}\right)\Phi^{(2)} + \left(V_1 - u_{3,2}^{\mathrm{C}}\right)\Phi^{(3)} + W_1(\Phi^{(1)} + \Phi^{(2)} + \Phi^{(3)}). \tag{24}$$

We remark that one obtains the original Schrödinger-type equation (8) by summing up the differential equation version of all equations in (22), and then using Eqs. (18)–(21). We also remark that Eq. (22) ensures that the component $\Phi^{(i)}$ is symmetric under exchange of particles j and k, and thus the total wave function Ψ, Eq. (19), is totally symmetric with respect to i, j, and k.

Here, we define a set of complete and orthogonal functions describing the angular parts of the three-body system with state index θ and the radial part of the spectator particle with momentum p,

$$|\mathcal{F}_\theta(p)) \equiv |\theta(\hat{\boldsymbol{x}}, \hat{\boldsymbol{y}})) \times \sqrt{\frac{2}{\pi}} \frac{F_\ell[\eta(p), py]}{y}, \tag{25}$$

where $F_\ell[\eta(p), py]$ is the regular Coulomb function:

$$[T_\ell(y) + u^{\mathrm{C}}(y)] F_\ell[\eta(p), py] = \left(\frac{3\hbar^2}{4m_\alpha} p^2\right) F_\ell[\eta(p), py], \tag{26}$$

with

$$T_\ell(y) = -\frac{3\hbar^2}{4m_\alpha}\left(\frac{d^2}{dy^2} - \frac{\ell(\ell+1)}{y^2}\right) \tag{27}$$

and a Coulomb parameter $\eta(p) = \frac{2m_\alpha}{3\hbar^2}\frac{2(Ze)^2}{p}$.

The function $\Phi^{(1)}(\boldsymbol{x}, \boldsymbol{y})$ thereby can be expanded as

$$\Phi^{(1)}(\boldsymbol{x}, \boldsymbol{y}) = \sum_\theta \int_0^\infty dp\, |\mathcal{F}_\theta(p)) \frac{\phi_\theta(x, p)}{x}, \tag{28}$$

where the function $\phi_\theta(x, p)$ is a solution of an ordinary differential equation:

$$[E_q - T_L(x) - V^{\mathrm{S}}(x) - V^{\mathrm{C}}(x)]\phi_\theta(x, p) = \omega_\theta(x, p) \tag{29}$$

with

$$E_q = \frac{\hbar^2}{m_\alpha} q^2 = E - \frac{3\hbar^2}{4m_\alpha} p^2 \tag{30}$$

and

$$T_L(x) = -\frac{\hbar^2}{m_\alpha}\left(\frac{d^2}{dx^2} - \frac{L(L+1)}{x^2}\right). \tag{31}$$

The source function $\omega_\theta(x, p)$ is given by

$$\omega_\theta(x, p) = x(\mathcal{F}_\theta(p)|H_{\gamma,1}\Psi_b + [\Delta\Phi]^{(1)}\rangle. \tag{32}$$

The boundary condition to get a physical solution of Eq. (29) depends on E_q and thus on the integral variable p in Eq. (28) via Eq. (30). According to the sign of E_q, the range of p ($0 \leqslant p < \infty$) is divided into two regions: (i) $0 \leqslant p \leqslant p_c = \sqrt{\frac{4m_\alpha}{3\hbar^2}E}$, where $E_q \geqslant 0$, and (ii) $p_c < p < \infty$, where $E_q < 0$. The corresponding boundary conditions are

$$\phi_\theta(x, p) \underset{x\to\infty}{\propto} \begin{cases} u_L^{(+)}[\gamma(q), qx] & (0 \leqslant p \leqslant p_c), \\ W_{-\gamma(|q|),L+1/2}(2|q|x) & (p_c < p < \infty), \end{cases} \tag{33}$$

where $u_L^{(\pm)}(\gamma, r)$ is defined as

$$u_L^{(\pm)}(\gamma, r) = e^{\mp\imath\sigma_L(\gamma)}\left[G_L(\gamma, r) \pm \imath F_L(\gamma, r)\right], \tag{34}$$

where $G_L(\gamma, r)$ is the irregular Coulomb function, the factor $\sigma_L(\gamma)$ is the Coulomb phase shift, $\gamma(q) = \frac{m_\alpha}{2\hbar^2}\frac{(Ze)^2}{q}$, and the function $W_{\kappa,\mu}(z)$ is the Whittaker function [29]. We solve Eq. (29) with the above conditions by applying the usual techniques as in the two-body problem, e.g., the Numerov algorithm [22,30].

The Faddeev component $\Phi^{(1)}(\boldsymbol{x}, \boldsymbol{y})$ has an asymptotic form similar to Eq. (9) with a breakup amplitude:

$$f^{(\mathrm{B})}(q, \hat{\boldsymbol{x}}, \hat{\boldsymbol{y}}) = e^{\frac{\pi}{4}\imath}\left(\frac{4K_0}{3}\right)^{3/2} \sum_\theta |\theta(\hat{\boldsymbol{x}}, \hat{\boldsymbol{y}})) \times \frac{\imath^{-L-\ell}}{p} \frac{m_\alpha/\hbar^2}{1 - \imath\mathcal{K}_L(q)} \langle\bar{\psi}_L(q)|\omega_\theta(p)\rangle, \tag{35}$$

where $\bar{\psi}_L(x; q)$ is an α-α scattering solution with the standing-wave boundary condition and $\mathcal{K}_L(q)$ is the scattering K matrix for two-body scattering (see Appendix C of Ref. [22]). The total breakup amplitude is thus obtained according to the Faddeev decomposition (19) as

$$F^{(\mathrm{B})}(q_1, \hat{\boldsymbol{x}}_1, \hat{\boldsymbol{y}}_1) = f^{(\mathrm{B})}(q_1, \hat{\boldsymbol{x}}_1, \hat{\boldsymbol{y}}_1) + f^{(\mathrm{B})}(q_2, \hat{\boldsymbol{x}}_2, \hat{\boldsymbol{y}}_2) + f^{(\mathrm{B})}(q_3, \hat{\boldsymbol{x}}_3, \hat{\boldsymbol{y}}_3). \tag{36}$$

III. CALCULATIONS

A. Remarks on three-body calculations

Here, we remark on the 3-α calculations. Some other technical remarks in solving the Faddeev equations for three-body

TABLE I. Potential parameters of the α-α potential, Eq. (37), for AB(A′) [35] and AB(D) [34] and calculated values of the ^{8}Be(0^+_1) resonance energy $E_{r,2\alpha}$ and width $\Gamma_{2\alpha}$. Empirical values are taken from Ref. [36].

Potential	AB(A′)	AB(D)	Empirical
a_R (fm)	1.53	1/0.70(∼1.4)	
$V_R^{(0)}$ (MeV)	125.0	500.0	
$V_R^{(2)}$ (MeV)	20.0	320.0	
a_A (fm)	2.85	1/0.475(∼2.11)	
V_A (MeV)	− 30.18	− 130.0	
$E_{r,2\alpha}$ (keV)	93.4	95.1	91.8
$\Gamma_{2\alpha}$ (eV)	8.59	8.32	5.57 ± 0.25

breakup reactions accommodating three-body potentials and Coulomb potentials are given in Refs. [21,22,31–33].

1. Interactions

We use the two-range Gaussian form [34] for the nuclear part of the α-α potential,

$$V^{\rm S}(x) = \hat{P}_{2\alpha,L} V_R^{(L)} e^{-(x/a_R)^2} + V_A e^{-(x/a_A)^2}, \qquad (37)$$

where $\hat{P}_{2\alpha,L}$ is a projection operator on the L angular momentum α-α state. In the present work, two different parameter sets will be used: one is from Ref. [35], which is a slightly modified version of model A of the Ali-Bodmer (AB) potential [34], AB(A′); the second set is model D of the AB potential, AB(D). Table I shows the parameters and calculated properties of α-α resonance in comparison with empirical values [36].

The α-α potentials used in this work are shallow and so do not support bound states. However, it is known (see, e.g., Refs. [37–39]) that the use of such shallow α-α potentials does not reproduce some 3-α observables, e.g., binding energies and resonance energies. In order to reproduce these observables, we introduce a 3BP, which depends on the total angular momentum of the 3-α system, which takes a form given in Ref. [35],

$$V_{3\alpha} = \sum_{J=0,2} \hat{P}_{3\alpha,J} W_3^{(J)} \exp\left(-\frac{A_\alpha R^2}{2b_3^2}\right), \qquad (38)$$

where $\hat{P}_{3\alpha,J}$ is a projection operator on the 3-α state with total angular momentum J, $A_\alpha = m_\alpha/m_N = 3.97$ and $b_3 = 3.9$ fm, and the strength parameters $W_3^{(J)}$ will be determined below.

2. Two-body singularity

In the integral representation of wave functions, Eq. (28), we need to take care of the existing ^{8}Be(0^+_1) resonance with energy $E_{r,2\alpha}$ and width $\Gamma_{2\alpha}$, which causes a rapid dependence of $\phi_\theta(x, p)$ on the variable p through Eq. (30). As an example, the function $\phi_\theta(x, p)$ for the inhomogeneous term in Eq. (22) at $x = 2.8$ fm and $E = 0.2$ MeV with the AB(D) potential is plotted as a function of E_q instead of p in Fig. 1. Here, we set about 30 p-mesh (equivalently, E_q-mesh) points for

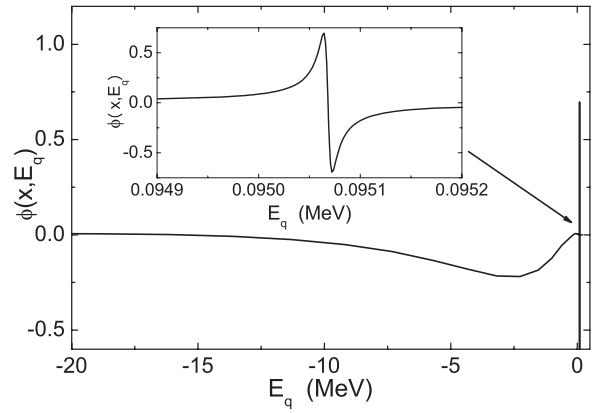

FIG. 1. The function $\phi_\theta(x, p)$ for the inhomogeneous term in Eq. (22) at $x = 2.8$ fm and $E = 0.2$ MeV with the AB(D) potential plotted as a function of E_q. The insertion is the magnified drawing of $\phi_\theta(x, p)$ around the 2-α resonance energy.

$E_{r,2\alpha} - 10\Gamma_{2\alpha} < E_q < E_{r,2\alpha} + 10\Gamma_{2\alpha}$. The function reveals a sharp E_q dependence around the ^{8}Be(0^+_1) resonance energy, which is safely treated by the condensed mesh points. Also, we remark that the effects of the function at negative E_q values, which correspond to a closed channel, are significant. Thus, in the present calculation, we choose the maximum value of the variable p as the one corresponding to $E_p \approx 160$ MeV.

3. Cutoff procedure

Here, we remark on the introduction of the auxiliary potentials. Besides the role of introducing the Coulomb distorted spectator function $F_\ell[\eta(p), py]$, Eq. (26), they have another role to play: In the integral kernel of Eq. (22), there appears $u^C_{2,3}(y_1)$ with a combination of the Coulomb potential acting on particles 2 and 3:

$$\left(\frac{1}{x_1} - \frac{1}{y_2}\right). \qquad (39)$$

As explained in Ref. [21], this term is supposed to be a short-range function with respect to the variable x_1 because of the cancellation between two terms, which makes the integral kernel tractable. However, while this cancellation holds sufficiently for bound states and continuum states below three-body breakup threshold, it does not hold sufficiently for the case of the three-body breakup reaction [22]. To avoid difficulties arising from this, we introduce a mandatory cutoff factor $e^{-(x/R_C)^4}$ to Eq. (39). This is an approximation made for this calculations. To check the convergence property of the cutoff range R_C, we performed calculations by changing the cutoff radius R_C, and we found that $R_C = 35$ fm is enough to obtain converged results.

4. Bound state

For the initial ^{12}C(2^+_1) state, we solve a homogeneous version of Eq. (22) [31] by taking into account 3-α partial wave states having 2-α states of the angular momentum up to 4 [37,38]. The strength parameter of the 3BP for the

TABLE II. The strength parameters of the three-body potential $W_3^{(2)}$ for the AB(A′) and AB(D) α-α potential modes together with calculated values of the binding energy of the $^{12}C(2_1^+)$ state, E_b. The empirical binding energy is taken from Ref. [40].

α-α model	$W_3^{(2)}$ (MeV)	E_b (MeV)
AB(A′)	−56.3	−2.840
AB(D)	−46.0	−2.830
Empirical		−2.8357

$J = 2$ state, $W_3^{(2)}$, is determined to reproduce the empirical binding energy of the $^{12}C(2_1^+)$ state [40]. The chosen values of $W_3^{(2)}$ for the AB(A′) and AB(D) α-α potentials are shown in Table II.

In solving the bound-state problem, it is enough to calculate wave functions within a rather restricted area, e.g., ($x \leqslant 12$ fm, $y \leqslant 80$ fm). However, to use the bound-state wave function in solving Eq. (22), we need to extend it to large values of the x and y variables. In actual calculation, we extend the bound-state wave function up to 100 fm for both of these variables. In the present calculations, the extension is performed by expanding the calculated wave function by using Gaussian functions. The previous results of the present author [18,19] were insufficient with respect to this expansion, and the present results below are updated, which causes a minor change.

5. *The x- and y-mesh points*

To solve the Schödinger-type equation (29), the solution $\phi_\theta(x, p)$ is connected to the asymptotic form of Eq. (33) at $x = 40$ fm in the present calculation. The function $\phi_\theta(x, p)$ is then extended up to $x = 1000$ fm by using the asymptotic form. By using these functions and Eq. (28), the wave function can be extended up to 1000 fm in the y variable. These maximum values in x and y variables are checked to give a converged result.

B. Numerical results

For calculations of 3-α continuum states with the $J = 0$ state, we take into account 3-α partial wave states of $(L, \ell) = (0, 0)$ and $(2, 2)$. The calculated photodisintegration cross sections reveal a sharp resonance corresponding to the Hoyle state. The strength parameter of the 3BP, $W_3^{(0)}$, is determined to reproduce the empirical resonance energy of the Hoyle state. Results for the combination with the AB(A′) and for the AB(D) potentials are listed in Table III, where truncated calculations with the $(L, \ell) = (0, 0)$ state are denoted by a subscript 0.

The partial decay width for the photoemission process, Γ_γ, and the 3-α decay width $\Gamma_{3\alpha}$, which is assumed to equal the total width, are evaluated by fitting the calculated cross sections around the Hoyle resonance with a Breit-Wigner formula:

$$\sigma_\gamma(E) = \frac{\pi}{10}\left(\frac{\hbar c}{E_\gamma}\right)^2 \frac{\Gamma_{3\alpha}\Gamma_\gamma}{(E - E_r)^2 + \Gamma_{3\alpha}^2/4}, \qquad (40)$$

TABLE III. Strength parameters of the 3BP for the 3-α 0^+ state, $W_3^{(0)}$, and calculated resonance parameters of the Hoyle state, $E_{r,3\alpha}$, $\Gamma_{3\alpha}$, and Γ_γ, for the Faddeev and CDCC calculations. See the text for the subscript 0 in the Faddeev calculation. Empirical values are taken from Ref. [40].

Calculation	$W_3^{(0)}$ (MeV)	$E_{r,3\alpha}$ (keV)	$\Gamma_{3\alpha}$ (eV)	Γ_γ (meV)
Faddeev				
AB(A′)	−96.2	376.966	9.1	1.8
AB(A′)$_0$	−168.0	377.929	9.5	2.7
AB(D)	−155.5	377.956	6.9	2.4
AB(D)$_0$	−305.5	376.724	6.4	2.9
CDCC				
AB(A′)	−315.0	381.241	126	4.7
Empirical		379.4	8.3 ± 1.0	3.7 ± 0.5

and these are also listed in Table III. The calculated photodisintegration cross sections are plotted in Fig. 2.

By adapting calculated photodisintegration cross sections to Eq. (6), the 3α reaction rates are obtained by numerical integrations. The cross sections are normalized to reproduce the empirical value of Γ_γ. This is essential to give a reaction rate that agrees with that of the NACRE rate in the resonant region, where the sequential process dominates the reaction and the 3α rate is proportional to Γ_γ (see, e.g., Eq. (15) of Ref. [6]).

Calculated 3α reaction rates, multiplied by the square of the Avogadro constant N_A by convention, for AB(A′) and AB(D) are shown in Fig. 3 as a function of temperature $T_7 = T/(10^7\ \mathrm{K})$. In the figure, reaction rates for NACRE, OKK, and HHR are also plotted for comparison. In Fig. 4, ratios of these calculations to the NACRE rate are shown.

Although Table III demonstrates that the determined values of $W_3^{(0)}$ depend on the truncation of the partial wave states, it turns out that calculated 3α reaction rates essentially do not change once the resonance energy is fitted. Actually, those calculations are indistinguishable even if plotted in Fig. 4.

Our results for the 3α reaction rate at higher temperatures $T_7 > 10$ agree with the NACRE rate within a few percent

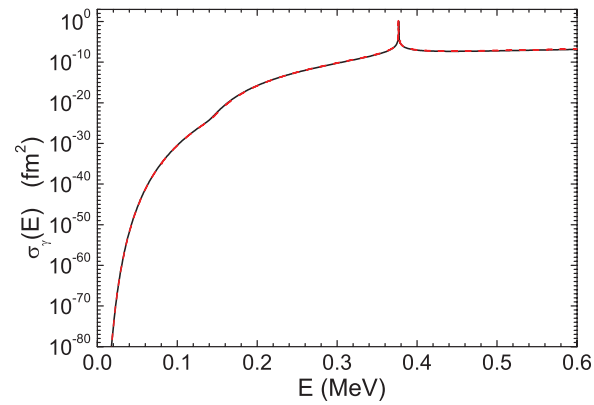

FIG. 2. (Color online) Calculated photodisintegration cross section for the process, Eq. (5), as a function of the 3-α energy E. The solid line is the result for AB(A′) and the dashed line is for AB(D).

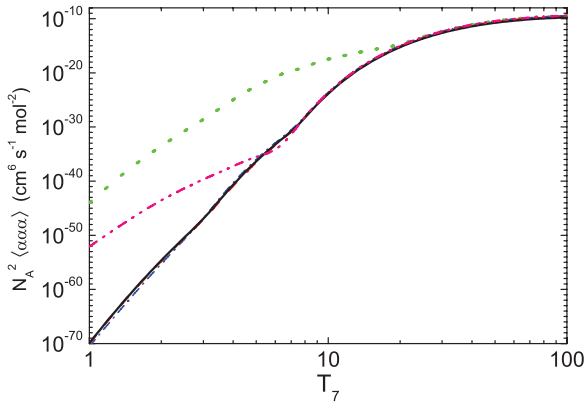

FIG. 3. (Color online) The 3α reaction rate as a function of temperature. The solid line denotes the present calculation for AB(A′), the dashed line is for AB(D), the dot-dashed line is the NACRE rate [5], the dotted line is the OKK rate [8], and the dot-dot-dashed line is the HHR rate [17].

owing to normalization of the photodisintegration cross section to reproduce the γ decay width of the Hoyle state. However, this contrasts with the calculations of Refs. [8,17], which need to be multiplied by an additional factor after the normalization. To see the contribution of the Hoyle state, the 3α rate is calculated by performing the integration of Eq. (6) just around the Hoyle state energy, i.e., in the limited range within 10 times the 3-α decay width. The result for AB(A′) is plotted in Fig. 4 as a thin solid line, which demonstrates that the reaction rate for $T_7 > 10$ is actually dominated by the Hoyle state.

At lower temperatures, the present results are slightly higher than the NACRE rate, which contradicts the OKK and HRR rates. While the present 3α rates for AB(A′) and AB(D) are about 10 times larger than the NACRE rate at $T_7 = 1$, the OKK (HHR) rate is about 10^{26} (10^{18}) times larger than the NACRE rate at the same temperature. These differences will be discussed in the next section.

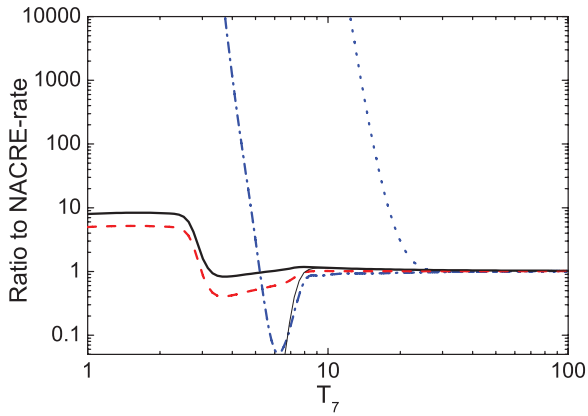

FIG. 4. (Color online) Ratio of the 3α reaction rates to the NACRE rate as a function of temperature. The solid and dashed lines denote the Faddeev calculations for AB(A′) and AB(D), respectively; the dotted line is for the OKK rate; the dot-dashed line is for the HHR rate; the thin solid line is the Hoyle state contribution for AB(A′) (see the text).

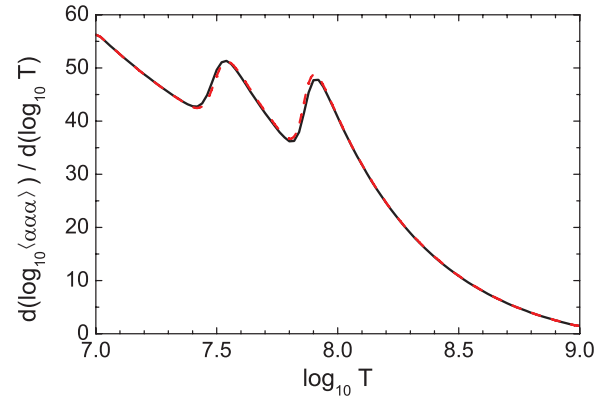

FIG. 5. (Color online) Temperature-dependent parameter $d\log_{10}\langle\alpha\alpha\alpha\rangle/d\log_{10} T$ calculated from the present 3α reaction rate. The solid and dashed lines denote the Faddeev calculations for AB(A′) and AB(D), respectively.

Recently, Suda *et al.* [14] studied constraints on the 3α reaction rate from stellar evolution theory. They obtained the following constraints: (i) $N_A^2\langle\alpha\alpha\alpha\rangle < 10^{-29}$ cm^6 s^{-1} mol^{-2} at $T \approx 10^{7.8}$ K ($T_7 \approx 6.1$); (ii) a temperature-dependent parameter $d\log_{10}\langle\alpha\alpha\alpha\rangle/d\log_{10} T \geqslant 10$ at $T_7 \approx$ (10–12). Figure 3 demonstrates that the present rate satisfies constraint (i). The temperature-dependent parameter calculated from the present result is plotted in Fig. 5, which shows that constraint (ii) is also satisfied for the present rates.

IV. DISCUSSION

A. CDCC calculation

In order to discuss the differences between the present Faddeev calculations and the OKK calculation for the 3α reaction rate in some detail, we will perform a CDCC calculation for the 3α process. However, while the CDCC method was applied to calculate the 3-α continuum states $|\boldsymbol{q}, \boldsymbol{p}\rangle^{(+)}$ in Ref. [8], it is applied to solve Eq. (8) in the present work.

In the CDCC method [41,42], a three-body wave function is expressed by a particular set of Jacobi coordinates, e.g., $(\boldsymbol{x}_1, \boldsymbol{y}_1)$, which will be designated as $(\boldsymbol{x}, \boldsymbol{y})$.

We divide the range of the q variable into small intervals of size Δq, called bins, $[q_{n-1}, q_n(= q_{n-1} + \Delta q)]$ $(n = 1, 2, \ldots, N_q)$. For each bin, we define a continuum discretized (CD) α-α base function by

$$\hat{\phi}_n(x) = \frac{1}{\sqrt{C_n}} \int_{q_{n-1}}^{q_n} dq\, w_n(q)\phi(x;q), \tag{41}$$

where $\phi(x;q)$ is the α-α scattering wave functions for the energy E_q,

$$[E_q - T_L(x) - V_1(x)]\phi(x;q) = 0, \tag{42}$$

$w_n(q)$ is a weight function [41,42], and C_n is the normalization factor,

$$C_n = \int_{q_{n-1}}^{q_n} dq\, |w_n(q)|^2 . \tag{43}$$

Here, we consider solving Eq. (8) by expanding the solution by the CD base restricting the $L = \ell = L_0 = 0$ partial wave state,

$$\Psi(\boldsymbol{x}, \boldsymbol{y}) = \frac{1}{4\pi} \sum_{n=1}^{N_q} \frac{\hat{\phi}_n(x)}{x} \frac{\hat{\psi}_n(y)}{y}, \tag{44}$$

which leads to a set of coupled equations,

$$\sum_{n'=1}^{N_q} [[E_{p_n} - T_\ell(y)]\delta_{n,n'} - \hat{V}_{n,n'}(y)]\hat{\psi}_{n'}(y) = \frac{y}{4\pi} \langle \hat{\phi}_n | H_\gamma | \Psi_b \rangle, \tag{45}$$

where

$$E_{p_n} = E - E_{q_n} \tag{46}$$

and

$$\hat{V}_{n,n'}(y) = \frac{1}{(4\pi)^2} \langle \hat{\phi}_n | V_2 + V_3 + W | \hat{\phi}_{n'} \rangle. \tag{47}$$

In calculating this coupling potential, we neglect the angular momentum dependence of the α-α potential to avoid any nonlocality, and we use the $L = 0$ component of the 2BP.

The boundary condition for the function $\hat{\psi}_n(y)$ depends on the energy of the spectator particle, E_{p_n}. For a positive energy state of the spectator, it is purely outgoing, e.g.,

$$\hat{\psi}_n(y) \underset{y\to\infty}{\to} u_0^{(+)}[\eta(p_n), p_n y]\mathcal{T}_n, \tag{48}$$

and then the photodisintegration cross section is given by

$$\sigma_\gamma = \frac{2}{45\pi} \frac{\hbar c}{mc^2} \sum_n{}' \frac{|\mathcal{T}_n|^2}{p_n}, \tag{49}$$

where the prime means that the summation over n is restricted within a range where $E_{p_n} \geqslant 0$.

In the present calculation, we use 120 averaged states by setting $q_0 = 0.010$ fm^{-1} ($E_{q_0} = 1.0$ keV) with $\Delta q = 0.001$ fm^{-1}, namely, $q_{120} = 0.130$ fm^{-1} ($E_{q_{120}} = 175$ keV), which is a choice similar to that of the OKK calculation: 122 states for $q_0 = 0.008$ fm^{-1} ($E_{q_0} = 0.608$ keV) to $q_{122} = 0.130$ fm^{-1} ($E_{q_{122}} = 176$ keV). Equation (45) is integrated up to $y_{\max} = 2500$ fm, and the obtained solutions are connected to the outgoing boundary conditions (48). In calculating the coupling potential (47), the CD-base functions are integrated up to $x_{\max} = 5000$ fm. These maximum values are the same as in the OKK calculations. We use the AB(A′) α-α potential. The same wave function as in the Faddeev calculation above is used for the initial 3-α ^{12}C(2_1^+) state using the AB(A′) model.

The strength parameter of the 3BP that is determined to reproduce the Hoyle resonance energy is shown in Table III.

Due to numerical difficulties in solving Eq. (45) when a channel with negative energy of E_{p_n} exists, in the present work, calculations are performed for $E \geqslant 250$ keV, where all CD channels involved in the calculations are open.

In Fig. 6, we plot results of the phododisintegration cross section by the solid line in comparison with the Faddeev result as denoted by the dashed line. As is expected, the CDCC cross sections are larger by several orders of magnitude compared to the Faddeev cross sections. The resonance parameters calculated by using the CDCC method are listed in Table III, which shows that the calculated width for 3-α decay in the CDCC calculations is 10 times larger than that of the Faddeev calculations and the empirical value.

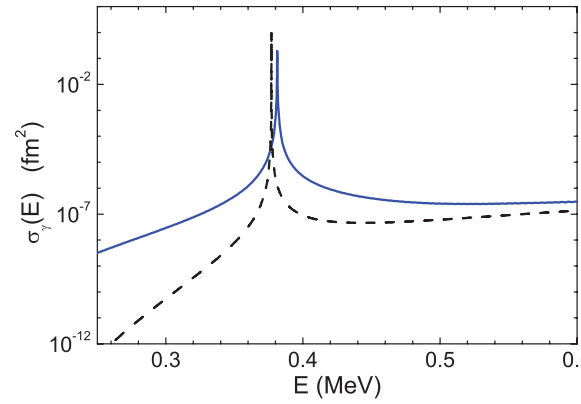

FIG. 6. (Color online) Photodisintegration cross sections of ^{12}C(2_1^+) calculated by using the CDCC method (solid line) and the Faddeev method (dashed line).

The calculated 3α reaction rate as a ratio to the NACRE rate is plotted in Fig. 7, together with those of the OKK and the AB(A′)-Faddeev calculations, which demonstrates that a similar reaction rate enhancement as for the OKK rate is observed for the present CDCC calculation.

B. Decay of the Hoyle resonance

The authors of Ref. [8] claimed that the significant increase of the OKK rate at low temperatures is due to effects of the direct capture reaction, which are enhanced by a proper reduction of the Coulomb barrier between a nonresonant α-α pair and the spectator α particle (see, e.g., Fig. 3 of Ref. [8]). To check the effect of the direct process in the inverse photodisintegration cross section, we extract the sequential cross section as a term of the momentum bin including the α-α resonant state from Eq. (49), and then we define the direct

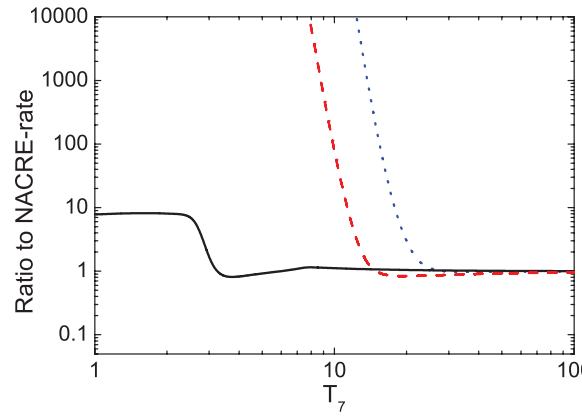

FIG. 7. (Color online) Ratio of the 3α reaction rates to the NACRE rate as a function of temperature. The solid line denotes the Faddeev calculations for AB(A′), the dashed line is the present CDCC calculation for AB(A′), and the dotted line is for the OKK rate.

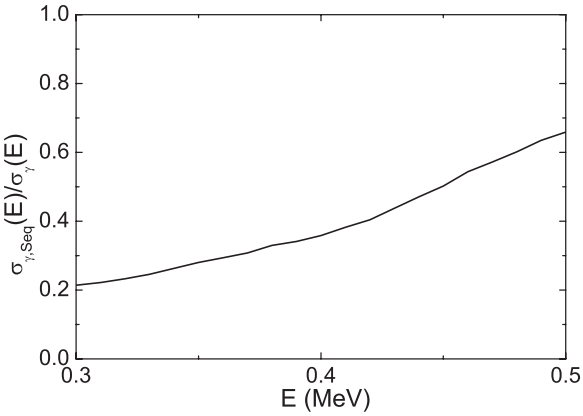

FIG. 8. Ratio of the resonant contribution to the phododisintegration cross section of the $^{12}C(2_1^+)$ state calculated by using the CDCC method for AB(A′).

cross section as the remaining portion. Figure 8 shows the ratio of the sequential cross section to the total cross section of the CDCC calculation for $0.3 \leqslant E \leqslant 0.5$ MeV. The figure shows that the contribution of the sequential cross section accounts for only a small fraction of the total. This implies a large contribution of the direct cross section and a reduction of the Coulomb barrier for the nonresonant 2-α state as mentioned above. In contrast to this, the sequential contribution for the Faddeev calculation defined as an integration around the 2-α resonance energy in Eq. (13) contributes more than 99% of the total cross section.

Here, we notice that the contribution of the sequential cross section in the present CDCC calculations becomes only about 30% of the total even at the Hoyle resonance energy. This tendency seems to contradict recent experimental results on the decay mechanism of the Hoyle state, which is produced in different ways: by $^{40}Ca + ^{12}C$ at 25 MeV/nucleon [43], by $^{10}C + ^{12}C$ at 10.7 MeV/nucleon [44], or by the $^{11}B(^3He, d)$ reaction at 8.5 MeV [45]. In these experiments, three α particles in the final state are measured in complete kinematics, from which a fraction of the sequential decay is extracted. While the authors of Ref. [43] obtained a rather small fraction, 83(±5)%, of the sequential decay, others [44,45] obtained a fraction of almost 100%. These results are consistent with the Faddeev calculations, but not with the CDCC calculations.

A possible reason for this difference may be related to the importance of rearrangement channels of the 3α reaction: Suppose that a pair of α particles, say 2 and 3, is in a nonresonant state. In the CDCC calculation, the third α particle, 1, feels a rather low Coulomb barrier compared to the case in which the pair is in the $^8Be(0_1^+)$ resonant state as shown in Fig. 3 of Ref. [8], and thus the direct reaction proceeds favorably to cause an enhancement of the 3α reaction rate. However, in the Faddeev formalism, because of a rearrangement reaction, another pair, say 1 and 3, can form a resonant state, and then the spectator, 2, feels a rather high Coulomb barrier, which can suppress the reaction. The CDCC calculations do not include such a coupling to rearrangement channels. As a result, we may say that the direct decay is enhanced for the CDCC calculation due to the lack of rearrangement channels.

Since the authors of Refs. [16,17] insist that the symmetrization of 3-α wave functions be explicitly taken into account in the HHR calculation, the above context may not apply to the difference between the present calculations and the HHR calculation. However, for further studies, it would be interesting to see how large the direct contribution in the HHR calculations can be.

V. SUMMARY

In this paper, calculations of the 3α reaction as a quantum mechanical three-body problem are performed. For this, a wave function corresponding to the inverse process is defined and solved by applying Faddeev three-body theory and accommodating the long-range Coulomb force effect.

Two different models of α-α potentials are used supplemented with 3-α potentials to reproduce the binding energy of the $^{12}C(2_1^+)$ state and the resonance energy of the Hoyle state. Our results for the 3α reaction rate are consistent with the NACRE rate at higher temperatures of $T_7 > 10$, where the sequential process is dominant, and are about 10 times larger at low temperature of $T_7 = 1$, although there exists a potential model dependence. However, our results contradict recent calculations obtained by using the CDCC and HHR methods, which exceed the NACRE rate by 10^{26} and 10^{18}, respectively, at $T_7 = 1$.

CDCC calculations for the three-body disintegration process have been performed, and results show a reaction rate enhancement similar to that for the OKK rate. We found that a significant difference between the Faddeev and the CDCC results exist in the contents of the decay of the Hoyle state: while sequential decay is dominant for the Faddeev calculation, it is only about 30% for the CDCC calculation, which contradicts recent experimental data for the decay of the Hoyle resonance.

[1] C. Tur, A. Heger, and S. M. Austin, Astrophys. J. **702**, 1068 (2009).
[2] H. O. U. Fynbo *et al.*, Nature (London) **433**, 136 (2005).
[3] E. E. Salpeter, Astrophys. J. **115**, 326 (1952).
[4] F. Hoyle, Astrophys. J. Suppl. **1**, 121 (1954).
[5] C. Angulo *et al.*, Nucl. Phys. A **656**, 3 (1999).
[6] E. Garrido, R. de Diego, D. V. Fedorov, and A. S. Jensen, Eur. Phys. J. A **47**, 102 (2011).
[7] K. Nomoto, F.-K. Thielemann, and S. Miyaji, Astron. Astrophys. **149**, 239 (1985).
[8] K. Ogata, M. Kan, and M. Kamimura, Prog. Theor. Phys. **122**, 1055 (2009).
[9] A. Dotter and B. Paxton, Astron. Astrophys. **507**, 1617 (2009).
[10] P. Morel, J. Provost, B. Pichon, Y. Lebreton, and F. Thévenin, Astron. Astrophys. **520**, A41 (2010).
[11] F. Peng and C. D. Ott, Astrophys. J. **725**, 309 (2010).

[12] M. Saruwatari and M. Hashimoto, Prog. Thoer. Phys. **124**, 925 (2010).
[13] Y. Matsuo, H. Tsujimoto, T. Noda, M. Saruwatari, M. Ono, M. Hashimoto, and M. Fujimoto, Prog. Thoer. Phys. **126**, 1177 (2011).
[14] T. Suda, R. Hirschi, and M. Y. Fujimoto, Astrophys. J. **741**, 61 (2011).
[15] Y. Kikuchi, M. Ono, Y. Matsuo, M. Hashimoto, and S. Fujimoto, Prog. Thoer. Phys. **127**, 171 (2012).
[16] N. B. Nguyen, F. M. Nunes, I. J. Thompson, and E. F. Brown, Phys. Rev. Lett. **109**, 141101 (2012).
[17] N. B. Nguyen, F. M. Nunes, and I. J. Thompson, arXiv:1209.4999.
[18] S. Ishikawa, Few-Body Syst. **54**, 479 (2013).
[19] S. Ishikawa, AIP Conf. Proc. **1484**, 257 (2012).
[20] L. D. Faddeev, Zh. Eksp. Teor. Fiz. **39**, 1459 (1961) [Sov. Phys. JETP **12**, 1041 (1961)].
[21] S. Ishikawa, Few-Body Syst. **32**, 229 (2003).
[22] S. Ishikawa, Phys. Rev. C **80**, 054002 (2009).
[23] K. Yabana and Y. Funaki, Phys. Rev. C **85**, 055803 (2012).
[24] K. Yabana (private communication).
[25] R. de Diego, E. Garrido, D. V. Fedorov, and A. S. Jensen, Eur. Phys. Lett. **90**, 52001 (2010).
[26] S. Ishikawa, H. Kamada, W. Glöckle, J. Golak, and H. Witała, Phys. Lett. B **339**, 293 (1994).
[27] T. Sasakawa and T. Sawada, Suppl. Prog. Theor. Phys. **61**, 61 (1977).
[28] T. Sasakawa and T. Sawada, Phys. Rev. C **20**, 1954 (1979).
[29] F. W. J. Olver, D. W. Lozier, R. F. Boisvert, and C. W. Clark, eds., *NIST Handbook of Mathematical Functions* (Cambridge University Press, New York, 2010).
[30] T. Sawada and T. Sasakawa, Sci. Rep. Tohoku Univ. Ser. 8 **4**, 1 (1983).
[31] T. Sasakawa and S. Ishikawa, Few-Body Syst. **1**, 3 (1986).
[32] S. Ishikawa, Nucl. Phys. A **463**, 145 (1987).
[33] S. Ishikawa, Few-Body Syst. **40**, 145 (2007).
[34] S. Ali and A. R. Bodmer, Nucl. Phys. **80**, 99 (1966).
[35] D. V. Fedorov and A. S. Jensen, Phys. Lett. B **389**, 631 (1996).
[36] D. R. Tilley, J. H. Kelley, J. L. Godwin, D. J. Millener, J. E. Purcell, C. G. Sheu, and H. R. Weller, Nucl. Phys. A **745**, 155 (2004).
[37] I. Filikhin, V. M. Suslov, and B. Vlahovic, J. Phys. G **31**, 1207 (2005).
[38] Z. Papp and S. Moszkowski, Mod. Phys. Lett. B **22**, 2201 (2008).
[39] Y. Suzuki, H. Matsumura, M. Orabi, Y. Fujiwara, P. Descouvemont, M. Theeten, and D. Baye, Phys. Lett. B **659**, 160 (2008).
[40] F. Ajzenberg-Selove, Nucl. Phys. A **506**, 1 (1990).
[41] M. Kamimura, M. Yahiro, Y. Iseri, Y. Sakuragi, H. Kameyama, and M. Kawai, Prog. Theor. Phys. Suppl. **89**, 1 (1986).
[42] N. Austern, Y. Iseri, M. Kamimura, M. Kawai, G. Rawitscher, and M. Yahiro, Phys. Rep. **154**, 125 (1987).
[43] A. R. Raduta *et al.*, Phys. Lett. B **705**, 65 (2011).
[44] J. Manfredi, R. J. Charity, K. Mercurio, R. Shane, L. G. Sobotka, A. H. Wuosmaa, A. Banu, L. Trache, and R. E. Tribble, Phys. Rev. C **85**, 037603 (2012).
[45] O. S. Kirsebom *et al.*, Phys. Rev. Lett. **108**, 202501 (2012).